Technique for frequency selective, sub-diffraction limited imaging of rare-earth ions in bulk crystals

John G. Bartholomew, Matthew J. Sellars

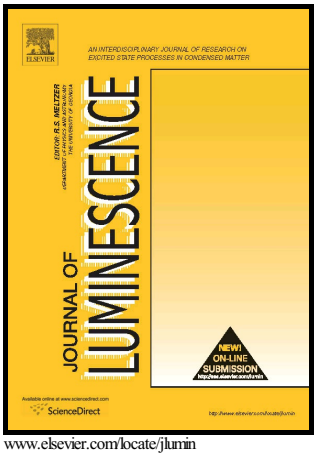

www.elsevier.com/locate/jlumin

PII: S0022-2313(17)31174-2
DOI: https://doi.org/10.1016/j.jlumin.2017.10.039
Reference: LUMIN15106

To appear in: *Journal of Luminescence*

Received date: 9 July 2017
Revised date: 13 October 2017
Accepted date: 14 October 2017

Cite this article as: John G. Bartholomew and Matthew J. Sellars, Technique for frequency selective, sub-diffraction limited imaging of rare-earth ions in bulk crystals, *Journal of Luminescence,* https://doi.org/10.1016/j.jlumin.2017.10.039

Technique for frequency selective, sub-diffraction limited imaging of rare-earth ions in bulk crystals

John G. Bartholomew[1,*], Matthew J. Sellars

Centre for Quantum Computation and Communication Technology, Laser Physics Centre, The Australian National University, Canberra, Australian Capital Territory 2601, Australia

Abstract

We propose and demonstrate the principle of a sub-diffraction-limited optical imaging technique for rare-earth ion crystals that preserves the ions' homogeneous line width. Our method uses a combination of applied electric field gradients and optical pumping to create a resonant nanoscopic volume within an otherwise non-resonant macroscopic crystal. We present the concept of the Stark activation technique and perform a demonstration in Pr^{3+}:Y_2SiO_5 in which we create a 10 μm-thick absorption feature in a 1 mm thick crystal. By modeling the system we show that it is possible to increase the resolution of the technique to the 5 nm range for single Pr^{3+} ions. We also discuss the physical properties that will fundamentally limit the resolution of Stark activation. Because the proposed technique simultaneously achieves high spatial and high spectral resolution it is an enabling protocol to realize technology based on single rare-earth ions and harness short-range interactions in ensembles.

Keywords: Rare-earth crystals, Stark effect, Superresolution.

*Corresponding author: john.g.bartholomew@gmail.com

[1]Current address: T. J. Watson Laboratory of Applied Physics, California Institute of Technology, 1200 E California Blvd, Pasadena, CA, 91125, USA

1. Introduction

The definitive optical detection of single rare-earth ions in crystalline hosts marked an important breakthrough for future classical and quantum technology using this class of materials. The success of several groups in this endeavor [1, 2, 3] opens up avenues to pursue the long-held aim to harness the unique optical and spin properties of rare-earth ion crystals at the single-ion level. In particular, achieving single-emitter resolution frees measurement and manipulation from the limiting effects of inhomogeneous broadening [4]. Without inhomogeneous broadening it is possible to enhance and extend the performance of protocols that are constrained in ensemble systems. For example, when ensembles in stochastically doped crystals are used as frequency-based qubits the size of the qubit network is fundamentally limited by inhomogeneities in the electric dipole-dipole interaction [5]. Applying the same architecture developed for ensembles to single ions removes the limitations of inhomogeneity and it is possible to significantly increase the number of interacting rare-earth ion qubits in a local network. To achieve this advance it is critical to address individual ions and to precisely control interactions between individual ions in rare-earth ion materials with narrow optical and spin transition homogeneous line widths.

One avenue for realizing a resource of interacting single rare-earth ion qubits is to develop methods that isolate single ions in bulk crystals. The aim of this strategy is to exploit the existing materials and ensemble-based techniques that have produced the narrowest optical and nuclear spin transition line widths in the solid state [6, 7]. The challenge associated with the bulk crystal approach is to achieve single ion resolution whilst preserving both the optical and spin transition homogeneous line widths. This requirement of preserving the best aspects offered in bulk crystals increases the difficulty of the already technically demanding task of single ion optical detection.

The $4f \leftrightarrow 4f$ optical transitions of rare-earth ions are only very weakly allowed [8]. The weakness of their oscillator strength provides the basis for very narrow resonances when cooled below 4 K (as low as $\approx$100 Hz [6]), but also extremely low emission rates (typically less than 10^4 photons per second). To detect the fluorescence from a narrow transition of a single ion requires simultaneously achieving high levels of collection efficiency, spatial resolution, background rejection, frequency resolution, and long term spatial and spectral stability [1, 2, 3, 9, 10].

Despite the progress made in single ion optical detection, there has been little development of techniques to allow a network of interacting single ions to be isolated, measured, and controlled in a bulk crystal, whilst preserving the narrow line widths of the optical and spin transitions. In this paper, we propose and explore a new technique that should allow this aim to be achieved. The technique is designed to selectively activate a sub-diffraction-limited volume within a bulk crystal, which enables single ion detection and preserves the ion's properties. Our method, Stark activation, uses a combination of applied electric field gradients and optical pumping to create a bright (resonant) state nanoscopic volume within a macroscopic crystal that is maintained in a dark

(non-resonant) state. Stark activation can be applied in the absence of closed optical transitions, which is the case for most rare-earth ion materials, and also if cyclic transitions exist [11, 12]. The technique also offers sub-diffraction limited imaging of ensembles. This versatility is valuable in experimental progress and development toward achieving the final goal of a small quantum network based on local interactions between single rare-earth ion qubits.

The paper is divided up into four further sections. First, an overview of some of the techniques that have successfully achieved single rare-earth ion detection is provided to establish the advantages of Stark activation. In Section 3 the concept of Stark activation is outlined and in Section 4 we present a proof-of-principle demonstration of the technique in one dimension on a 10-micron scale. This is followed in Section 5 by a discussion of the potential resolution and applications for Stark activation imaging, which extend into both the single ion and ensemble regimes. Stark activation allows a combination of selectively addressing bulk crystals in sub-diffraction-limited spatial resolution and high frequency resolution. In doing so, it provides a way to analyze and utilize interactions that govern the properties of rare-earth ions in crystals in previously unattainable spatial detail.

2. Background: single rare-earth ion optical detection

There has been significant advances in the field of single rare-earth ion optical detection since the early experiments by Lange *et al.* on Sm^{2+}:CaF_2 in 1988 [13]. Although there have been many publications examining rare-earth ion materials close to the single ion regime [14, 15, 16, 17, 18], the focus in this section is on the work where either photon anti-bunching or a high degree of spectral statistical fine structure have been demonstrated.

To achieve high signal-to-noise ratio optical detection of a single rare-earth ion the spatial-spectral density within the collection volume must be sufficiently low. To determine what density is low enough it is necessary to consider not only the focus of the collection volume but its entirety. It is clearly desirable to have only one resonant ion within the collection volume focus. In addition, the integrated signal from resonant ions throughout the entire collection volume has to be considered to prevent a large background obscuring the single ion fluorescence.

There have been several demonstrations where only a single resonant ion is present in the entire collection volume [1, 2, 9]. This is possible by using nano-, sub-micron, or micron scale crystals to define the collection volume rather than the optical imaging system. The use of such crystals is an effective way to achieve high collection efficiency [2] and excellent background suppression [1]. The disadvantage of crystallite samples is that the homogeneous line widths of optical transitions in such systems have been measured to be in excess of 10^3 times broader than those achieved in bulk crystals [9]. Although significant progress is currently being made to grow nanoparticles with narrow homogeneous line widths [19, 20], bulk crystals still offer the best performance for storage and manipulation of quantum states.

To capitalize on the narrow homogeneous lines offered in rare-earth ion materials below 4 K, it is likely that bulk crystal systems are the best choice. To isolate a single ion in a macroscopic sample, the spatial-spectral density must be extremely low if the collection volume is defined by diffraction limited optics. As an example, for a single ion to be spatially isolated within a diffraction limited volume the density required is of the order of 10^{12} cm^{-3}. This ion density is equivalent to a dopant concentration of approximately 1 part in 10^{11}, which is difficult to attain even in high quality, nominally undoped host crystals [1]. Even in such ultra-pure crystals the background signal due to ions outside the collection focus increases significantly [1]. Furthermore, at this dopant concentration the average separation between ions is on the order of 600 nm. Such large separations would severely limit the ability to create a resource of interacting qubits. An alternative to using ultra-low concentration doped-samples is to engineer a lattice of isolated ions through implantation [1, 21]. Although an appealing prospect for creating scalable rare-earth ion architectures for quantum devices, the implantation technique has not yet reached a level where the narrow line widths found in as-grown samples can be achieved.

Making use of frequency space reduces the requirements on the spatial density. Tuning the laser frequency to the wings of the inhomogeneous distribution allows the spatial-spectral density to be very low in spite of high dopant concentrations. This is the strategy used in Ref. [3] in which the fluorescence of single Pr^{3+} ions is detected in a bulk 0.05% Pr^{3+}:LaF_3 crystal. The signature statistical fine structure of single ions was achieved at a frequency offset of 100 GHz from the center of the inhomogeneously broadened transition (FWHM = 13 GHz). Although Ref. [3] demonstrates the feasibility of this strategy there are two significant disadvantages. First, the ions that are resonant at frequencies in the wings of the inhomogeneous distribution reside in sites with significantly different crystalline environments to those in the center of the distribution (particularly at a frequency offset of 10 times the inhomogeneous line width). This may lead to significantly different physical properties including hyperfine interactions [22] and homogeneous line widths [23]. Second, a search in frequency space is required to find an offset where the spatial-spectral density is suitable. This is because the inhomogeneously broadened line in rare-earth crystals do not, in general, obey simple Lorentzian or Gaussian distributions [24]. Once a suitable frequency offset is identified, an additional search is required to find single ion signals. When signal acquisition is slow due to the long integration times needed for sufficient signal-to-noise ratio detection, performing such searches places stringent conditions on long term spatial and spectral stability.

Developing techniques to probe bulk rare-earth ion crystals in spatial resolution beyond the diffraction limit offers another avenue toward single ion optical detection in a network of interacting ions. To date, two methods have been applied to achieve super-resolution in rare-earth doped materials. The first was a modified stimulated emission depletion (STED) technique, which harnessed upconversion to achieve 54 nm resolution in Pr^{3+}:YAG nanoparticles [25]. The second technique used pointillistic image analysis to localize a single Pr^{3+} ion in a Y_2SiO_5 nanocrystal to within 5 nm [2]. Both methods offer excellent res-

olution enhancement compared to the diffraction limit however, both possess disadvantages for probing small ensembles of single-ion qubits. Applying STED on a $4f \leftrightarrow 4f$ transition through upconversion to a $5d$ level can significantly enhance the emission rate of a single ion but at the expense of broadening the narrowest line width of the initial transition. The disadvantage of pointillistic methods is that two resonant ions separated by less than the diffraction limit cannot be resolved.

Super-resolution imaging based on reversible saturable optical linear fluorescence transitions (RESOLFT) including STED without upconversion, and ground state depletion (GSD) [26, 27, 28] are well suited to rare-earth ions because of their long lived ground state spin levels [29, 6]. In this work we draw upon the use of a long-lived shelving state whilst defining the spatial resolution with electric field gradients rather than optical intensity gradients. By Stark shifting the ions, rather than applying multiple laser frequencies, the available frequency space is used more efficiently. Furthermore, Stark activation avoids the repeated optical pumping preparation that would be required in all-optical methods and hence, allows higher signal levels in situations where no closed optical transitions exist (see Section 5.1). The method of Stark activation is designed to create a resonant nanoscopic region within a bulk sample. By defining a sub-λ^3 volume within a bulk crystal, rather than through the use of a nanocrystal, it should be possible to access the narrowest possible homogeneous line widths available in rare-earth crystals without sacrificing background rejection. Furthermore, because the potential resolution is a significant enhancement compared to the diffraction limit, single ion investigations are not restricted to ions in extremely dilute samples or in highly strained sites. Thus, combining our technique with the high collection efficiency, high frequency stability, and low noise apparatus used for current single ion techniques offers a different regime for studies at the single ion level.

3. Stark activation for super-resolution

The Stark activation technique is specifically designed to take advantage of the narrow homogeneous line widths, long spin state lifetimes, and linear Stark interaction in rare-earth ion crystals. Fig. .1 illustrates how these factors can be combined to achieve high spatial resolution through the application of a large electric field gradient in a bulk crystal. By exciting the bulk crystal at a single optical frequency, all resonant ions will be optically pumped to a non-resonant ground state hyperfine level. Because the lifetime of these hyperfine levels can be of the order of minutes [29] to days [6], the ions that are initially optically excited will be maintained in the dark state. To bring the ions in the dark state back into resonance with the laser, an electric field can be applied to Stark shift the transition such that

$$\mathrm{E} \cdot \delta\mu = \Delta E \ , \tag{1}$$

where E is the applied electric field, $\delta\mu$ is the difference in the electric dipole moment between the ground and excited state levels, and ΔE is the ground state hyperfine splitting energy.

The resonant condition of Eq. 1 can be made spatially dependent if an electric gradient is applied such that

$$\mathrm{E}(r) \cdot \delta\mu = \Delta E, \text{ for some } r. \tag{2}$$

By alternating between zero field and the applied field gradient, only the Stark activated region will be maintained in a bright state, whilst all other ions are non-resonant. Therefore, Stark activation allows a region within a bulk crystal to continually fluoresce under single-frequency excitation, whilst the rest of the crystal is maintained in a dark state. In Sec. 5 we show that the spatial definition of the bright state region ultimately depends on the homogeneous line width Γ_{h}, the ground state hyperfine splitting ΔE, and the applied electric field gradient. Given the sub-kHz optical line widths, hyperfine splittings of the order of 10s of MHz, and the electric field gradients achievable with micron-scale electrodes, it is feasible to realize a sub-diffraction-limited bright-state region within a bulk sample.

The concept of Stark activation is very similar to magnetic resonance imaging (MRI) techniques, where a magnetic field gradient is used to create a spatially defined resonance criterion [30, 31]. Indeed, there have been proposals and implementations of such techniques for imaging in solid-state materials [32, 33, 34, 35, 36]. Such nano-MRI are unsuitable in this case because specific static magnetic fields must be applied to attain the minimum decoherence on the rare-earth spin state transitions [37]. Similar techniques that use Stark interactions to define the resonance criterion have been proposed in rare-earth ion crystals [38] and have also demonstrated sub-diffraction-limited resolution in molecular imaging [39, 40, 41]. The cited techniques rely either on having only a very small number of emitters in the collection volume, or on the inhomogeneous line width of the transition being narrow compared to experimentally achievable transition frequency shifts. The uniqueness of Stark activation is that super-resolution can be achieved in high density bulk samples without requiring a Stark interaction greater than the inhomogeneous line width. As such, Stark activation is suitable for a broad range of rare-earth ion materials and applications.

4. Proof-of-principle demonstration

The aim of the following experiment was to demonstrate the feasibility of super-resolution spatial selectivity in a bulk rare-earth ion crystal. This initial work was designed to show the ability of Stark activation to isolate an optical section that was thin compared to the depth of the sample, but in a regime with a high signal level. The demonstration involved preparing an inhomogeneously

broadened absorption feature within a transparent spectral region through optical pumping that was dependent on the electrical field gradient (see Fig. .2(b)). To achieve a sufficiently high signal level in our system we relaxed the frequency resolution of the technique, which correspondingly increased the spatial extent of the bright state region. To achieve the full resolution of Stark activation imaging requires a modified pulse sequence, which is shown in Fig. .2(d) and discussed in Section 5.1.

The apparatus for the experiment is shown in Fig. .2(a). A 40 μm diameter copper wire electrode was stretched across 0.05% Pr^{3+}:Y_2SiO_5 crystal, which was mounted on the cold finger of a continuous flow liquid helium cryostat. To ensure good thermal contact between the sample and the cold finger at 4.6 K, the crystal was fixed in place by partial immersion in molten indium. The sample was spectroscopically probed in the region of the electrode through an objective microscope lens (NA = 0.7), which was configured as part of a home built confocal microscope. To excite the $^3H_4 \leftrightarrow {}^1D_2$ optical transition of the praseodymium dopants, a ring dye laser, frequency stabilized to less than 1 kHz, was tuned to a frequency of approximately 494.725 THz (606 nm). Pulses were generated and intensity stabilized using a series of double pass acousto-optic modulator set-ups, and delivered to the confocal microscope through a single mode optical fiber. The emission from the sample at wavelengths greater than 611 nm was separated from the excitation laser wavelength using two high pass, reflective filters. This emission was collected with a single mode fiber, which also acted as the confocal pinhole, and detected on a single photon resolving avalanche photodiode (APD). The combined collection and detection efficiency of the system was approximately 1%, which included the loss due to the shadow cast by the electrode. The reflected light at the excitation wavelength was collected in a single mode fiber, which was also confocal to the imaging focus, and detected with a photomultiplier tube (PMT). This allowed the reflected laser light from the sample surface to be used as a position reference in the z direction.

An optical pumping sequence (see Fig. .2(b) and (c)) was used to demonstrate the principal of the Stark activation technique. A 4 MHz spectral trench was prepared by optically pumping all resonant ions to non-resonant hyperfine ground states with a high intensity (100 nW of power) frequency sweep. During this burn sequence the voltage on the electrode was held at 0 V. A 1 MHz wide absorption feature was then optically pumped into the center of the trench using Stark activation. To create this feature the laser was scanned rapidly over 1 MHz at a power of 30 nW whilst 26 V (RP_1) and then -42.5 V (RP_2) were applied to the electrode, each with a duration of 10 ms. The repumping voltages RP_1 and RP_2 were optimized using separate hole burning measurements to produce an electric field that resulted in a linear Stark shift of 10.2 MHz and -17.3 MHz, respectively, at a distance of 235 ± 20 μm from the axis of the wire electrode: a depth of 5 μm below the crystal surface. The resultant absorption feature was then measured by monitoring the fluorescence from the sample during a 100 ms scan over 4 MHz at a power of less than 10 nW. The feature width is dominated by the inhomogeneous broadening resulting from the 1 MHz

excitation bandwidth, which is of the order of 50 times larger than the measured homogeneous line width at this temperature (18±0.7 kHz). This sequence was repeated many times to accumulate enough photon counts for sufficiently high signal-to-noise data.

We probed the depth of Stark activated region by repeating the measurement at different z positions of the objective focus. The integrated photon counts as a function of frequency and depth are shown in Fig. .3. The projection of the Stark activated feature onto the depth axis shows that the fluorescence decreases significantly as the collection region moves away from a depth of 5 μm. Importantly, when the focus of the lens is 10 μm below the sample surface, corresponding to 5 μm away from the region where the Stark activation is optimized, the fluorescence level decreases to approximately one quarter of the maximum value. In contrast, if the absorption feature is prepared optically but without Stark activation, the fluorescence level increases as the focus moves deeper into the crystal because more ions are contributing to the signal. The definitive decrease of the fluorescence in Fig. .3 highlights that the resonance condition is being controlled by the interaction between the ions and the electric field produced by the electrode rather than the optical field. Therefore, by using the Stark activation technique we have created a resonant layer of ions of the order of 10 μm thick within a crystal of 1 mm thickness.

5. Discussion

The basic implementation of Stark activation presented in the previous section demonstrates the ability of the technique to spatially isolate ions in a large bulk crystal. In this section we discuss how to apply Stark activation to achieve single ion isolation, and investigate the limits of the technique to highlight the significant improvements that can be made to progress from this simplistic demonstration to super-resolution spatial selectivity. A model is proposed to describe the resolution of the current experiment and used to suggest improvements to the experiment using the same electrode and crystal. Third, the ultimate resolution limit is discussed by considering alternative electrode geometries and other rare-earth ion materials. Finally, we briefly present some applications of the Stark activation imaging technique.

5.1. From proof-of-principle to imaging

Part (d) of Fig. .2 shows the sequence to extend Stark activation to the single ion level. The sequence contains a single preparation step, where all resonant ions are optically pumped to a non-resonant ground state, and a Stark activation step. The main differences between this sequence and the one described in Section 4 are that the laser frequency remains fixed throughout the sequence, the signal is acquired during the Stark activation step, and the timing of the sequence has changed. The laser frequency is fixed so that only a narrow frequency region is prepared and activated. During the Stark activation step, the ion will emit a photon each time the applied voltage brings a transition

from the populated ground state into resonance with the laser. The length of the preparation and Stark activation steps are related to the lifetime T_1 of the optical transition. The preparation step should have a duration of the order of $10T_1$ but only needs to be performed once. The duration of each individual applied voltage in the Stark activation step should be of the order of T_1, and Stark activation can continue for as long as required. The signal level achievable for a single Pr^{3+} ion in Y_2SiO_5 is expected to be of the order of 100 counts/s. This is based on the study of single Pr^{3+} ions in Ref. [9], where multiple laser frequencies were used to maintain the ion in a resonant state rather than the Stark shifting proposed here. In contrast, an all optical method, such as GSD, would require a preparation step before each readout step, which would result in a comparatively small signal level.

5.2. Model of Stark activation resolution

The next part of the discussion focuses on developing a model to analyze the spatial resolution possible with the Stark activation technique. The frequency shift Δ_f due to the linear Stark interaction arising from a voltage V applied to a long, cylindrical electrode of radius a whose axis is a distance d above the surface of a rare-earth ion crystal can be approximated by

$$\Delta_f \propto \frac{SV}{((b+z)^2+x^2)^{\frac{1}{2}}} \ , \tag{3}$$

where S is the linear Stark coefficient, $b=\sqrt{d^2-a^2}$, x is the lateral distance from the electrode axis, and z is the depth below the crystal surface.

At the location where Δ_f is equal to the hyperfine frequency splitting $\Delta_{\mathrm{HF}} = \Delta E/h$, the first order derivatives of the Δ_f with respect to position, Stark coefficient, and voltage are

$$\frac{\partial \Delta_f}{\partial x} = \Delta_{\mathrm{HF}} \frac{-x}{(b+z)^2+x^2} \ , \tag{4a}$$

$$\frac{\partial \Delta_f}{\partial z} = \Delta_{\mathrm{HF}} \frac{(b+z)}{(b+z)^2+x^2} \ , \tag{4b}$$

$$\frac{\partial \Delta_f}{\partial S} = \Delta_{\mathrm{HF}} \frac{1}{S} \ , \tag{4c}$$

$$\frac{\partial \Delta_f}{\partial V} = \Delta_{\mathrm{HF}} \frac{1}{V} \ . \tag{4d}$$

Equations 4c and 4d define the change in the Stark shift with respect to the inhomogeneity in S and to the stability of the applied voltage V. Both of these

terms bound the frequency resolution of the Stark activation technique:

$$\delta f_S = \Delta_{\mathrm{HF}} \frac{\delta S}{S} \quad , \tag{5a}$$

$$\delta f_V = \Delta_{\mathrm{HF}} \frac{\delta V}{V} \quad . \tag{5b}$$

We define $\delta f_{\mathrm{total}}$ to be the total frequency resolution bound, which incorporates δf_S, δf_V, the optical excitation bandwidth, and the inhomogeneous broadening of the hyperfine level transitions Γ_{spin}. To achieve high spatial resolution the voltage stability should be sufficiently high to ensure that $\delta f_V \ll \delta f_{\mathrm{total}}$. Under such conditions, $\delta f_{\mathrm{total}}$ will be limited by δf_S, Γ_{spin}, and the homogeneous line width Γ_{h}. The contributions of these three limits on the resolution of Stark activation will be discussed later in this section, using the specific example of Pr^{3+}:Y_2SiO_5.

For a region to undergo Stark activation, the change in Stark shift defined by position δf_x and δf_z must be less than or equal to $\delta f_{\mathrm{total}}$, where

$$\delta f_x = \delta x \left(\Delta_{\mathrm{HF}} \frac{-x}{(b+z)^2 + x^2} \right) \quad , \tag{6a}$$

$$\delta f_z = \delta z \left(\Delta_{\mathrm{HF}} \frac{(b+z)}{(b+z)^2 + x^2} \right) \quad . \tag{6b}$$

Therefore, the spatial resolution of this configuration of the Stark activation technique in two dimensions is given by

$$\delta x \quad \leq \quad \frac{\delta f_{\mathrm{total}}}{\Delta_{\mathrm{HF}}} \frac{\left((b+z)^2 + x^2\right)}{x} \tag{7}$$

$$\delta z \quad \leq \quad \frac{\delta f_{\mathrm{total}}}{\Delta_{\mathrm{HF}}} \frac{\left((b+z)^2 + x^2\right)}{(b+z)} \quad . \tag{8}$$

In systems where it is necessary to apply more than one voltage to maintain fluorescence (if the relevant ions possess a spin greater than 1/2), the condition $\delta f_x, \delta f_z \leq \delta f_{\mathrm{total}}$ must hold for all frequency shifts. Because of this, the resolution of the Stark activation technique is set by the largest Stark shift required to maintain fluorescence.

Using Eq. 8 we have estimated the depth of the optical section created by the apparatus described in Sec. 4. In this case $\delta f_{\mathrm{total}}$ was dominated by the optical excitation bandwidth defined by the frequency width of the absorption feature (1 MHz). Given that the larger hyperfine splitting was 17.3 MHz, at a location relative to the wire defined by $x = 0$ μm, $b = 230$ μm, and $z = 5$ μm, the model gives a $\delta z = 13 \pm 2$ μm. This is in good agreement with the FWHM of the absorption feature obtained in the measurement.

5.3. Improvements to the current apparatus

There are several ways in which the spatial resolution of the technique could be improved, even using this simple apparatus. First, a significant increase in resolution is possible by reducing the excitation bandwidth below 1 MHz. For imaging ensembles the limit on the excitation bandwidth is δf_{total}, which has a contribution from δf_S and Γ_{spin}. For Pr^{3+}:Y_2SiO_5 it is highly likely that δf_{total} is dominated by Γ_{spin}, which is of the order of 100 kHz in zero field [29]. Although $\delta S/S$ is yet to be directly measured for rare-earth ion materials, this relative inhomogeneity can be bounded to the order of 0.1% by considering how the crystal field impacts S (see our further discussion in Appendix 6). By employing Stark activation with δf_{total} set to 100 kHz, $\delta z \approx 1.4$ μm, even for the electrode suspended 230 μm above the sample surface.

Second, because the frequency resolution of Stark activation is likely to be determined by Γ_{spin}, the spatial resolution can be increased by increasing the value of Δ_{HF}. In the initial experiment, we treated the $^1D_2$ excited state as a single energy level, whereas, just like the $^3H_4$ ground state, it has three doubly-degenerate hyperfine levels. By Stark activating one, rather than three, of the nine sub-ensembles resonant at any one frequency within the inhomogeneous line, Δ_{HF} can be increased to 36.9 MHz. This would decrease δz to 650 nm.

Third, the electric field gradient is significantly larger when the distance between the Stark activated region and the electrode is reduced. In particular, when the electrode is placed in contact with the surface of the crystal ($b = 0$). For the current electrode (40 μm diameter) the value of x must be sufficiently large such that the electrode is not significantly reducing the collection efficiency. By setting $x = 50$ μm, the resolution at a depth of 5 μm beneath the sample surface is $\delta x \approx 140$ nm and $\delta z \approx 1.4$ μm. This resolution would reflect the dipole moment of the praseodymium ions being oriented approximately along the x axis.

Fig. .4 shows a finite element model for the Stark activated regions for an infinitely long, 40 μm diameter wire electrode in contact with the surface of a Pr^{3+}:Y_2SiO_5 sample. In this case, a single sub-ensemble is activated with the larger value of Δ_{HF} set at 22.1 MHz: an intermediate regime between the proof-of-principle demonstration in Sec. 4 and the largest possible value of Δ_{HF}. The Y_2SiO_5 crystal is oriented such that the C_2 crystal axis is parallel with the electrode axis, and the D_1 and D_2 axes [29] are parallel to the horizontal and vertical axes, respectively. The shaded regions show the spatial extent of the Stark activated volumes for an excitation bandwidth of 1 MHz. There are two regions for each voltage because there are two inequivalent Stark subgroups in this configuration. As mentioned earlier, only the regions that can be optically accessed unimpeded by the electrode are useful from the perspective of a confocal microscope geometry. If δf_{total} is reduced to the level of 100 kHz, the Stark activated region has a characteristic width that is approximately ten times thinner than the shaded region, which corresponds to 100 nm-scale resolution in the x direction.

Thus far, the discussion of the resolution limit for Stark activation has been limited to ensembles, where inhomogeneity sets the lower bound on δf_{total}. In

the case where a single ion is isolated within the Stark activated region it is possible to further increase the resolution of the technique. This is because the lower bound on $\delta f_{\mathrm{total}}$ is free from inhomogeneities and hence, is set by the rate of spectral diffusion or, in the limit of negligible long term frequency drifts, the homogeneous line width Γ_{h}. To obtain the increased spatial resolution it would be necessary to measure both the Stark coefficient S and the hyperfine splittings of that particular ion. Although technically challenging, both measurements are possible. For example, S could be measured by adding an offset voltage to the electrode and determining the shift in laser frequency required to regain fluorescence. In the single ion regime other contributions to $\delta f_{\mathrm{total}}$ such as electrode voltage instability and laser frequency stability, must be small compared to Γ_{h}.

A single ion in bulk Pr^{3+}:Y_2SiO_5 possesses a homogeneous line width $\Gamma_h \approx 3$ kHz [42]. In the regime where $\delta f_{\mathrm{total}}$ is limited by Γ_{h}, the predicted resolution for an electrode configuration such as that in Figure .4 is $\delta x < 5$ nm and $\delta z \approx 40$ nm.

5.4. Further improvements to Stark activation resolution

The simple model presented above shows that the resolution of this imaging technique is governed by the electric field gradient, hyperfine ground state splitting, or equivalently the required Stark shift to achieve activation, and $\delta f_{\mathrm{total}}$. These parameters dictate the ultimate resolution of the Stark activation protocol. Therefore, our model indicates that by moving to other rare-earth ion crystals and a different electrode geometry, it is feasible to dramatically increase the spatial resolution. An example of another rare-earth ion crystal that possesses favorable properties for Stark activation imaging is Eu^{3+}:Y_2SiO_5: $\Gamma_{\mathrm{spin}} \approx 40$ kHz [43], $\Delta_{\mathrm{HF}}(\mathrm{max}) = 660$ MHz, and $\Gamma_h = 212$ Hz [6]. Compared to Pr^{3+}:Y_2SiO_5, the Eu^{3+}-doped crystal should allow an improvement in resolution by a factor of the order of 40 for ensembles and a factor up to 250 for single ions. It should be noted that although greater spatial resolution can be achieved, the use of Eu^{3+}:Y_2SiO_5 has the disadvantage of a lower emission rate from the activated volume compared to Pr^{3+}:Y_2SiO_5.

In general, the implementation of Stark activation can benefit from enhancing the optical emission rate through coupling the ions to photonic crystal cavities [44, 45]. The use of Purcell enhancement offers a higher photon flux, however, like the comparison between Pr^{3+} - and Eu^{3+} -doped Y_2SiO_5 above, ultimately there is a tradeoff between emission rate and resolution. This is because the additional radiative broadening will increase the ion's homogeneous linewidth.

A different electrode geometry also offers a potential increase in Stark activation resolution. For example, by depositing a planar electrode on the surface of the crystal the ions could be probed within 1 μm of the electrode in a region of very high electric field gradient without sacrificing collection efficiency. Using such an electrode to image ensembles in Pr^{3+}:Y_2SiO_5 is predicted to have a maximum spatial resolution of approximately 5 nm if the assumptions of our model remain valid. It is possible that due to the large applied electric field gradients in this regime higher order multipole terms such as the electric quadrupole will

become significant. The ultimate position resolution will then depend on the scale of these terms and the accuracy to which they can be determined.

Although the electrode geometry we have considered throughout this paper only provides an increase in resolution in two dimension, Stark activation is simply extended to a three dimensional super-resolution technique. The only change required is to change the electrode geometry from a wire or strip to a tip or point, such as those electrodes used in Refs. [39, 41].

5.5. Applications of Stark activation

Being able to examine any material in a previously unattainable regime provides a firm platform for enhanced understanding of physical interactions and technological development. The main motivation and obvious application for Stark activation is to spatially isolate single ions in bulk crystals. The advantage of Stark activation compared to other super-resolution techniques is that it allows narrow homogeneous line widths to be preserved, and the density of rare-earth ions can be high. For example, a Stark activated volume of 100 nm×100 nm×100 nm in a 0.05% Pr^{3+}:Y_2SiO_5 crystal would contain, on average, less than 250 ions. Assuming an inhomogeneously broadened distribution with center f_0 and a line width of 10 GHz, on average a single ion would be resonant within 40 MHz of f_0.

Because Stark activation preserves narrow line widths in super-resolution, it is also a suitable technique to study interactions between individual ions on nm-length scales. Interactions of interest for creating a network of entangled frequency qubits include electric dipole-dipole coupling, higher order electric multipole interactions, direct energy transfer, and exchange interactions. Detailed knowledge of these interactions in the solid state would be invaluable to future schemes for quantum information processing.

The applications of sub-diffraction-limited spatial resolution are not limited to technology at the single ion level. There are also interesting regimes in ensemble systems that Stark activation would assist in uncovering. One example is the study of crystals where ion-ion interactions have a greater strength than the hyperfine level splitting. In crystals, such as stoichiometric materials, where the introduction of a defect can create correlations between an ions resonant frequency and its proximity to the defect, the Stark activation technique could be used to study dipole-blockade mechanisms [46] and probe inhomogeneous broadening mechanisms at an unprecedented length-scale. Both interactions are highly important to future uses of rare-earth materials in non-linear quantum optics and high bandwidth quantum communication networks.

6. Conclusion

In this paper we have proposed and demonstrated an imaging technique to allow the properties of rare-earth ion crystals to be harnessed at a nanometer scale. The Stark activation technique takes advantage of the properties of rare-earth ions in the solid state, making it possible to create a nanoscale bright-state

region within an otherwise dark macroscopic crystal. The proposed technique provides an effective solution to isolating single rare-earth ions in regions of relatively high spatial-spectral density in bulk crystals. This allows the narrow line widths of the ions to be preserved and provides a foundation to investigate small networks of interacting frequency qubits based on single ions. A proof-of-principle experiment was performed in which we created a 10 μm thick optical section at the surface of 1 mm thick Pr^{3+}:Y_2SiO_5 crystal. A simple model of the experiment agrees well with the observed results and suggests that extensions of this work could achieve spatial resolution less than 10 nm. By combining the high spatial resolution possible by applying Stark activation with the already high spectral resolution offered by rare-earth ion crystals, there are many opportunities for exploring new regimes of physics in both the single ion and ensemble regimes.

This work was supported by the Australian Research Council Centre of Excellence for Quantum Computation and Communication Technology (CE110001027). M.J.S. was supported by an Australian Research Council Future Fellowship (FT110100919).

Appendix A: Upper bound on $\delta S/S$

It is possible to bound the relative inhomogeneity $\delta S/S$ by considering the relationship between the electric dipole moment and the crystal field [47]. Variations in S in an ensemble are due to the inhomogeneity in $(\mu_e - \mu_g)$, where the μ are the electric dipole moments for the excited and ground states, respectively. A conservative upper bound on $\delta S/S$ is then deduced by estimating the relative inhomogeneity in the individual μ_i: the ratio of the optical inhomogeneous broadening Γ_{ih} (of the order of 7 GHz in the sample studied in this work) to the separation between crystal field levels Δ_{cf} (of the order of 3 THz = 100 cm^{-1} [42]).

In addition to the above theoretical consideration, the estimate of $\delta S/S \approx 0.1\%$ is consistent with previously reported experimental results in which the linear Stark shift was applied in Pr^{3+}:Y_2SiO_5. In particular, in Ref. [48], the linear Stark shift was applied to realize the gradient echo quantum memory protocol. For the protocol to achieve an efficiency consistent with the model based on the optical absorption [49], $\delta S/S$ must be small compared to the ratio of the edge sharpness of the initial feature to the total broadening achieved by the linear Stark gradient. For the experiments in Ref. [48], the frequency half-width of the edges of the initial absorption feature were 12 kHz and the total Stark broadening was approximately 1.6 MHz. This suggests that $\delta S/S$ is small compared to 0.75%.

References

[1] R. Kolesov, K. Xia, R. Reuter, R. Stöhr, A. Zappe, J. Meijer, P. R. Hemmer, J. Wrachtrup, Optical detection of a single rare-earth ion in a crystal., Nat. Commun. 3 (2012) 1029.

[2] T. Utikal, E. Eichhammer, L. Petersen, A. Renn, S. Götzinger, V. Sandoghdar, Spectroscopic detection and state preparation of a single praseodymium ion in a crystal, Nat. Commun. 5 (2014) 3627.

[3] I. Nakamura, T. Yoshihiro, H. Inagawa, S. Fujiyoshi, M. Matsushita, Spectroscopy of single Pr^{3+} ion in LaF_3 crystal at 1.5 K, Sci Rep. 4 (2014) 7364.

[4] W. E. Moerner, M. Orrit, Illuminating Single Molecules in Condensed Matter, Science 283 (1999) 1670–1676.

[5] N. Ohlsson, R. K. Mohan, S. Kröll, Quantum computer hardware based on rare-earth-ion-doped inorganic crystals, Opt. Commun. 201 (2002) 71 – 77.

[6] F. Könz, Y. Sun, C. W. Thiel, R. L. Cone, R. W. Equall, R. L. Hutcheson, R. M. Macfarlane, Temperature and concentration dependence of optical dephasing, spectral-hole lifetime, and anisotropic absorption in Eu^{3+}:Y_2SiO_5, Phys. Rev. B 68 (2003) 085109.

[7] M. Zhong, M. P. Hedges, R. L. Ahlefeldt, J. G. Bartholomew, S. E. Beavan, S. M. Wittig, J. J. Longdell, M. J. Sellars, Optically addressable nuclear spins in a solid with a six hour coherence time, Nature (London) 517 (2015) 177.

[8] M. F. Reid, Transition intensities, in: G. Liu, B. Jacquier (Eds.), Spectroscopic Properties of Rare Earths in Optical Materials, Springer Berlin Heidelberg, 2005.

[9] E. Eichhammer, T. Utikal, S. Götzinger, V. Sandoghdar, Spectroscopic detection of single Pr^{3+} ions on the $^3H_4$ – $^1D_2$ transition, New J. Phys. 17 (2015) 083018.

[10] J. Karlsson, L. Rippe, S. Kröll, A confocal optical microscope for detection of single impurities in a bulk crystal at cryogenic temperatures, Rev. Sci. Instrum. 87 (2016) 033701.

[11] M. Afzelius, M. U. Staudt, H. de Riedmatten, N. Gisin, O. Guillot-Noël, P. Goldner, R. Marino, P. Porcher, E. Cavalli, M. Bettinelli, Efficient optical pumping of Zeeman spin levels in Nd^{3+}:YVO_4, J. Lumin. 130 (2010) 1566–1571.

[12] J. G. Bartholomew, R. L. Ahlefeldt, M. J. Sellars, Engineering closed optical transitions in rare-earth ion crystals, Phys. Rev. B 93 (2016) 014401.

[13] R. Lange, W. Grill, W. Martienssen, Observation of Single Impurity Ions in a Crystal, EPL 6 (1988) 499–503.

[14] S. M. Jaffe, M. L. Jones, W. M. Yen, Observation of dilution line narrowing in Eu^{3+}:SiO_2, J. Lumin. 60-61 (1994) 417–421.

[15] M. D. Barnes, A. Mehta, T. Thundat, R. N. Bhargava, V. Chhabra, B. Kulkarni, On-Off Blinking and Multiple Bright States of Single Europium Ions in Eu^{3+}:Y_2O_3 Nanocrystals, J. Phys. Chem. B 104 (2000) 6099–6102.

[16] A. P. Bartko, L. A. Peyser, R. M. Dickson, A. Mehta, T. Thundat, R. Bhargava, M. D. Barnes, Observation of dipolar emission patterns from isolated Eu^{3+}:Y_2O_3 doped nanocrystals: new evidence for single ion luminescence, Chem. Phys. Lett. 358 (2002) 459–465.

[17] Y. V. Malyukin, A. A. Masalov, P. N. Zhmurin, Single-ion fluorescence spectroscopy of a Y_2SiO_5:Pr^{3+} nanocluster, Phys. Lett. A 316 (2003) 147–152.

[18] Y. V. Malyukin, A. A. Masalov, P. N. Zhmurin, New fluorescence dynamics of a single Y_2SiO_5:Pr^{3+} nanocrystal, Opt. Commun. 239 (2004) 409–414.

[19] A. Perrot, P. Goldner, D. Giaume, M. Lovrić, C. Andriamiadamanana, R. R. Gonçalves, A. Ferrier, Narrow Optical Homogeneous Linewidths in Rare Earth Doped Nanocrystals, Phys. Rev. Lett. 111 (2013) 203601.

[20] J. G. Bartholomew, K. de Oliveira Lima, A. Ferrier, P. Goldner, Optical Line Width Broadening Mechanisms at the 10 kHz Level in Eu^{3+}:Y_2O_3 Nanoparticles, Nano Letters (2017) 778–787.

[21] K. Xia, R. Kolesov, Y. Wang, P. Siyushev, R. Reuter, T. Kornher, N. Kukharchyk, A. D. Wieck, B. Villa, S. Yang, J. Wrachtrup, All-Optical Preparation of Coherent Dark States of a Single Rare Earth Ion Spin in a Crystal, Phys. Rev. Lett. 115 (2015) 093602.

[22] R. L. Ahlefeldt, A. Smith, M. J. Sellars, Ligand isotope structure of the optical $^7F_0 \rightarrow {}^5D_0$ transition in $EuCl_3 \cdot 6H_2O$, Phys. Rev. B 80 (2009) 205106.

[23] R. M. Macfarlane, R. M. Shelby, Sub-kilohertz optical linewidths of the $^7F_0 \leftrightarrow {}^5D_0$ transition in Y_2O_3: Eu^{3+}, Opt. Commun. 39 (1981) 169–171.

[24] A. M. Stoneham, Shapes of inhomogeneously broadened resonance lines in solids, Rev. Mod. Phys. 41 (1969) 82–107.

[25] R. Kolesov, R. Reuter, K. Xia, R. Stöhr, A. Zappe, J. Wrachtrup, Superresolution upconversion microscopy of praseodymium-doped yttrium aluminum garnet nanoparticles, Phys. Rev. B 84 (2011) 153413.

[26] S. W. Hell, M. Kroug, Ground-state-depletion fluorscence microscopy: A concept for breaking the diffraction resolution limit, Appl. Phys. B 497 (1995) 495–497.

[27] S. Bretschneider, C. Eggeling, S. W. Hell, Breaking the Diffraction Barrier in Fluorescence Microscopy by Optical Shelving, Phys. Rev. Lett. 98 (2007) 218103.

[28] J. G. Bartholomew, Investigation of the scalability of rare-earth-ion quantum hardware, Ph.D. thesis, Australian National University, 2014.

[29] K. Holliday, M. Croci, E. Vauthey, U. P. Wild, Spectral hole burning and holography in an Y_2SiO_5:Pr^{3+} crystal, Phys. Rev. B 47 (1993) 14741–14752.

[30] P. Mansfield, P. K. Grannell, NMR 'diffraction' in solids?, J. Phys. C 6 (1973) L422–426.

[31] P. C. Lauterbur, Image formation by induced local interactions: example employing nuclear magnetic resonance, Nature (London) 242 (1973) 190–191.

[32] S. Schiller, R. L. Byer, Subwavelength Optical Magnetic-Resonance-Imaging, J. Opt. Soc. Am. A 9 (1992) 683–699.

[33] G. Balasubramanian, I. Y. Chan, R. Kolesov, M. Al-Hmoud, J. Tisler, C. Shin, C. Kim, A. Wojcik, P. R. Hemmer, A. Krueger, T. Hanke, A. Leitenstorfer, R. Bratschitsch, F. Jelezko, J. Wrachtrup, Nanoscale imaging magnetometry with diamond spins under ambient conditions, Nature 455 (2008) 648–651.

[34] C. Shin, C. Kim, R. Kolesov, G. Balasubramanian, F. Jelezko, J. Wrachtrup, P. R. Hemmer, Sub-optical resolution of single spins using magnetic resonance imaging at room temperature in diamond, J. Lumin. 130 (2010) 1635–1645.

[35] M. S. Grinolds, P. Maletinsky, S. Hong, M. D. Lukin, R. L. Walsworth, A. Yacoby, Quantum control of proximal spins using nanoscale magnetic resonance imaging, Nat. Phys. 7 (2011) 7.

[36] M. S. Grinolds, M. Warner, K. De Greve, Y. Dovzhenko, L. Thiel, R. L. Walsworth, S. Hong, P. Maletinsky, A. Yacoby, Subnanometre resolution in three-dimensional magnetic resonance imaging of individual dark spins, Nat. Nanotechnol. 9 (2014) 279–284.

[37] E. Fraval, M. J. Sellars, J. J. Longdell, Method of Extending Hyperfine Coherence Times in Pr^{3+}:Y_2SiO_5, Phys. Rev. Lett. 92 (2004) 5–8.

[38] J. H. Wesenberg, K. Mølmer, L. Rippe, S. Kröll, Scalable designs for quantum computing with rare-earth-ion-doped crystals, Phys. Rev. A 75 (2007) 012304.

[39] J. M. Segura, G. Zumofen, A. Renn, B. Hecht, U. P. Wild, Tip-induced spectral dynamics of single molecules, Chem. Phys. Lett. 340 (2001) 77–82.

[40] M. Bauer, L. Kador, Electric-field effects of two-level systems observed with single-molecule spectroscopy, J. Chem. Phys. 118 (2003) 9069–9072.

[41] S. Karotke, A. Lieb, B. Hecht, Stark-shift microscopy of single emitters, Appl. Phys. Lett. 89 (2006) 023106.

[42] R. W. Equall, R. L. Cone, R. M. Macfarlane, Homogeneous broadening and hyperfine structure of optical transitions in Pr^{3+}:Y_2SiO_5., Phys. Rev. B 52 (1995) 3963–3969.

[43] A. Arcangeli, M. Lovrič, B. Tumino, A. Ferrier, P. Goldner, Spectroscopy and coherence lifetime extension of hyperfine transitions in $^{151}Eu^{3+}$:Y_2SiO_5, Phys. Rev. B 89 (2014) 184305.

[44] T. Zhong, J. M. Kindem, E. Miyazono, A. Faraon, Nanophotonic coherent lightmatter interfaces based on rare-earth-doped crystals, Nature Communications 6 (2015) 8206.

[45] T. Zhong, J. Rochman, J. M. Kindem, E. Miyazono, A. Faraon, High quality factor nanophotonic resonators in bulk rare-earth doped crystals, Optics Express 24 (2016) 536.

[46] R. L. Ahlefeldt, M. R. Hush, M. J. Sellars, Ultranarrow Optical Inhomogeneous Linewidth in a Stoichiometric Rare-Earth Crystal, Physical Review Letters 117 (2016) 250504.

[47] R. M. Macfarlane, Optical Stark spectroscopy of solids, J. Lumin. 125 (2007) 156–174. (specifically, p. 160).

[48] M. P. Hedges, J. J. Longdell, Y. Li, M. J. Sellars, Efficient quantum memory for light, Nature 465 (2010) 1052–1056.

[49] G. Hétet, J. J. Longdell, A. L. Alexander, P. K. Lam, M. J. Sellars, Electro-Optic Quantum Memory for Light Using Two-Level Atoms, Phys. Rev. Lett. 100 (2008) 023601.

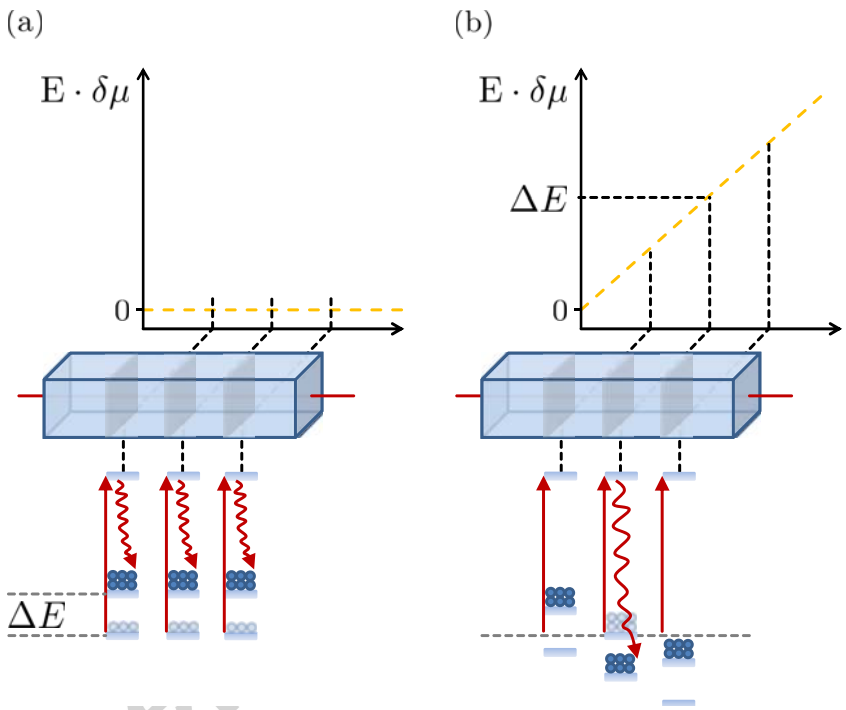

Figure .1: The concept for achieving high spatial resolution using the Stark activation technique. (a) A crystal is excited with a single frequency laser, which optically pumps all resonant ions to a non-resonant ground state: the dark state. (b) By applying an electric field gradient a small fraction of the crystal can be activated to fluoresce once more. The region is defined where the Stark shift equals the ground state energy splitting: $\mathrm{E} \cdot \delta\mu = \Delta E$.

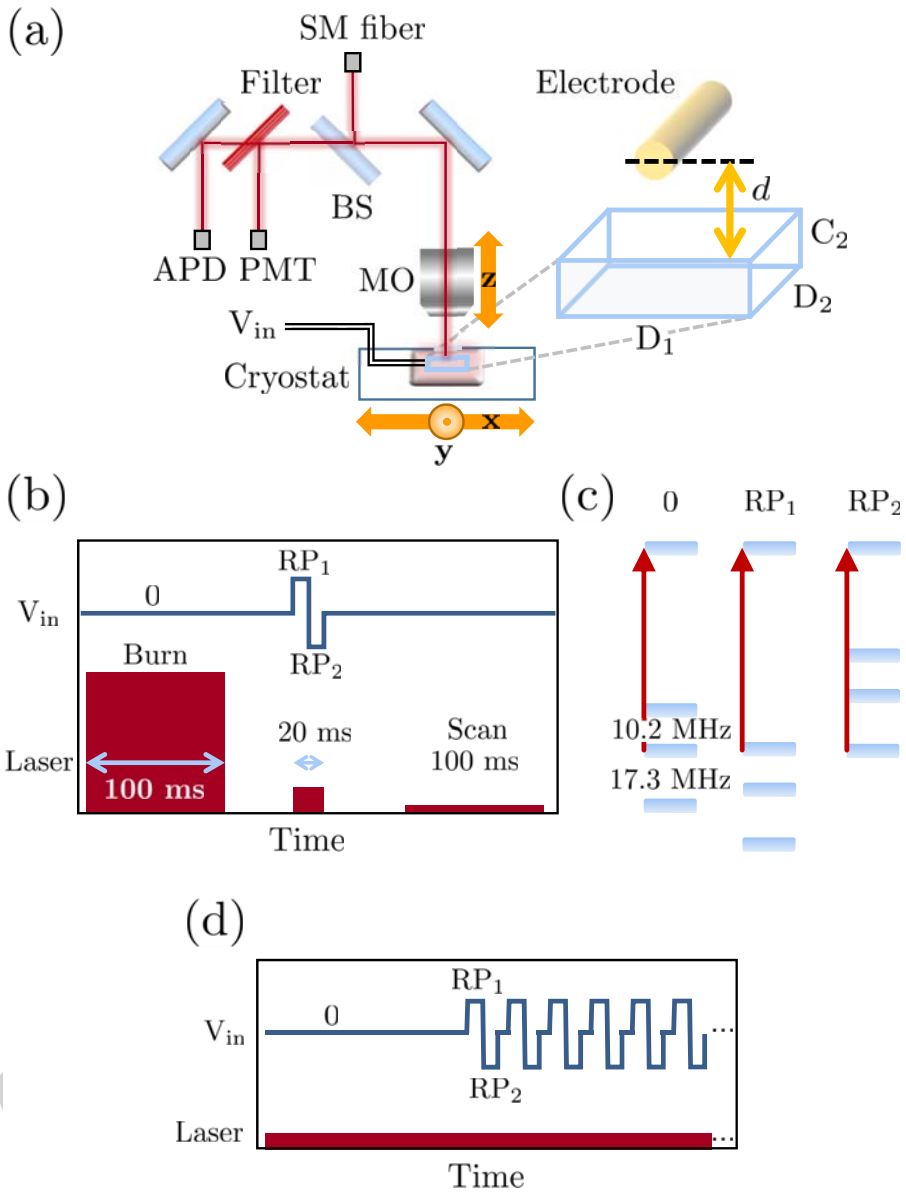

Figure .2: (a) Confocal microscope apparatus for high spatial resolution spectroscopy at 4 K (SM = single mode optical fiber, MO = microscope objective, and BS = beam splitter). (b) Pulse sequence for the proof-of-principle demonstration of Stark activation based on optically pumping. (c) The transition subgroups resonant for each applied voltage in the sequence in (b). Because the optical pumping sequence in this case was independent of the excited state hyperfine levels we draw only one of the three levels. (d) An indicative pulse sequence for achieving single ion isolation through Stark activation. Further details are provided in the text.

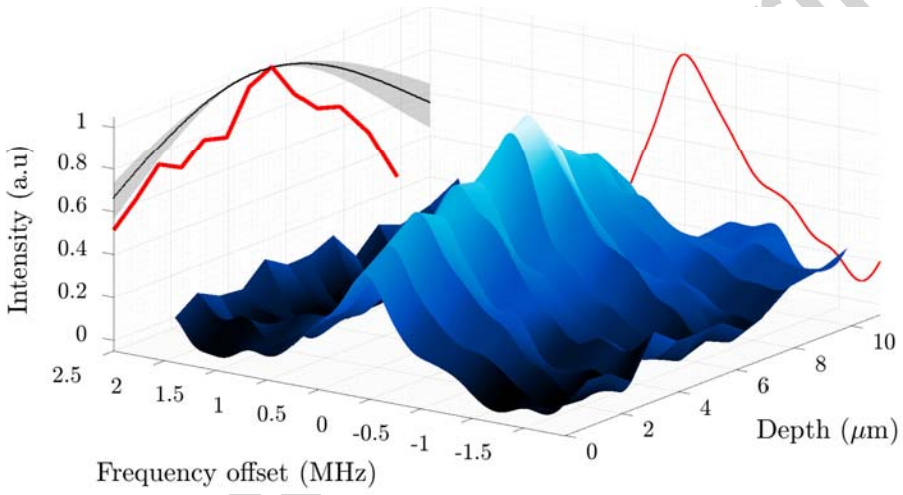

Figure .3: The 10 μm thick absorption region produced by the Stark activation method within a 1 mm thick Pr^{3+}:Y_2SiO_5 crystal. The resolution achieved is consistent with the model of the system, which predicts a resolution of 13±2 μm (the shaded trace accompanying the data on the Depth - Intensity axis).

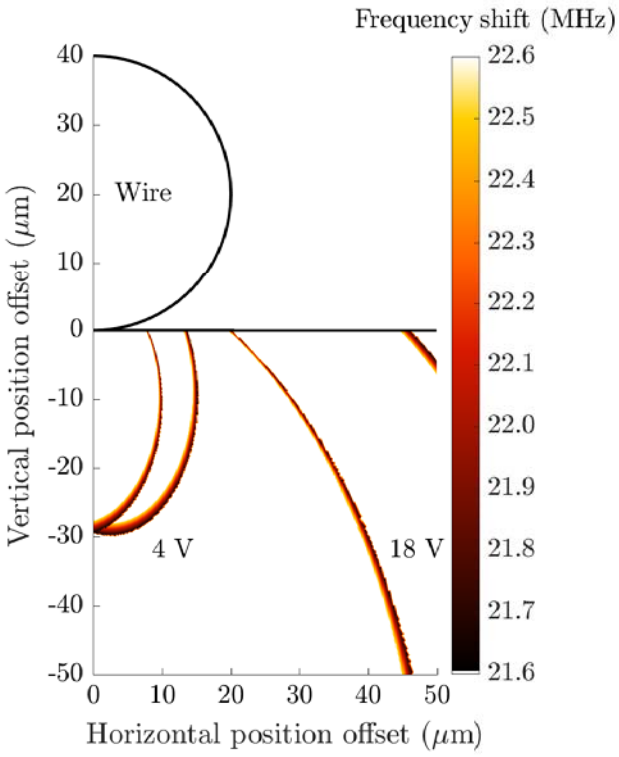

Figure .4: Finite-element model highlighting the spatial resolution of the Stark activation method. The shaded regions (color online) show the locations of ions that have a 22.1±0.5 MHz shift for 4 V or 18 V applied to the electrode. It is evident from the figure that the δz and δx near the surface approach or surpass the diffraction limit, particularly for a frequency bandwidth less than 100 kHz.